On the surface tension role in bubble growth and detachment in a micro-tube

Lynda Boubendir, Salah Chikh, Lounès Tadrist

On the surface tension role in bubble growth and detachment in a micro-tube

L. Boubendir[1], S. Chikh[1], L. Tadrist[2]

[1] USTHB, Faculty of Mechanical and Process Engineering, LTPMP, 16111 Algiers, Algeria

[2] Aix Marseille Université, CNRS, Laboratoire IUSTI, UMR 7343, 13453 Marseille, France

Abstract

The role of surface tension in the mechanism of bubble growth and detachment for a co-flowing air-water two-phase flow in a micro-tube is addressed. A numerical investigation for a horizontal axisymmetric flow with the assumption of zero gravity and an upward flow accounting for gravity contribution is carried out. The continuous liquid phase is flowing in a tube of 500 μm inner diameter and the gas phase is axially injected through a nozzle of 110 μm inner diameter and 210 μm outer diameter. A single-fluid model is used to determine the flow field, solving the continuity and momentum equations associated with the volume of fluid method for interface tracking. An open source software, OpenFOAM, is utilized for solving numerically this problem. The prediction results show that the surface tension plays a double role. First, it keeps the bubble attached to the injection nozzle during bubble growth and neck formation. Then, it destabilizes the interface by pinching off the neck in the immediate vicinity of the nozzle at about a distance of 0.5 the nozzle diameter rather than right at the nozzle exit. In-depth analysis of the mechanism of bubble formation induced by the effect of surface tension is carried out. It is highlighted that this latter acts as an attachment force at the injection nozzle during the bubble growth and it acts over the entire interface of the bubble yielding the formation of a neck. Later, the capillary effects reduce the diameter of the neck until it breaks and yields the detachment of the bubble. Further investigation at the nozzle wall allows depicting the motion of the contact line during the process of bubble growth and its significant effect on the bubble formation.

Keywords: Microfluidics two-phase flow, bubble formation, bubble detachment, surface tension, contact line.

Nomenclature

C_D drag coefficient

D tube diameter (m)

F_{AM} added mass force (N)

F_B buoyancy force (N)

F_D drag force (N)

F_M gas momentum force (N)

F_P pressure force (N)

F_S surface tension force (N)

g terrestrial gravitational acceleration

L tube length (m)

L_b nozzle length (m)

L_B bubble length (m)

$\vec{n}$ unit vector normal to the interface

P pressure (Pa)

Q volumetric flow rate (m^3/s)

r coordinate in radial direction (m)

R radius (m)

R_B bubble radius (m)

R_{bi} inner radius of nozzle (m)

R_{bo} outer radius of nozzle (m)

R_0 contact line radius (m)

R_N neck radius (m)

Re Reynolds Number ($\rho UD/\mu$)

S_B bubble surface (m^2)

t time (s)

u velocity (m/s)

U superficial velocity (m/s)

V_B bubble volume (m^3)

y coordinate in axial direction(m)

Y_{CM} Bubble center of gravity

Greek Symbols

γ_g Gravity level

φ volume fraction

κ curvature of the interface

μ dynamic viscosity (Pa .s)

ρ density (kg/m^3)

σ surface tension (N/m)

Θ contact angle (°)

τ viscous stress tensor, (Pa)

Subscripts

G or g gas

i phase

L or l liquid

LS liquid superficial

GS gas superficial

1. Introduction

Bubble formation from orifices in a liquid has been a topic of interest to the scientific community for several decades. It is mainly due to the wide variety of applications and processes in which this phenomenon is encountered like gas-liquid reactors, direct contact heat exchangers, flotation processes, etc. Recent developments in the field of two-phase microfluidics and processes in micro-reactors gave rise to renewed significant interest among the researchers (Wu and Gidaspow (2000), Günther and Jensen (2006), Garstecki et al. (2006), Shuietal (2007), Prakash and Gershenfeld (2007)).

This subject is still relevant because it is considered a fundamental process for understanding the interfacial phenomena. In several applications related to two-phase flow, it is important to predict the size of the bubbles formed to evaluate heat and mass transfer between phases and pressure loss in two-phase flows.

A literature review related to the formation and detachment of bubbles reveals that the majority of previous works dealt mostly with the same configuration of an upward gas flow through an orifice in a liquid at rest. This configuration is generally chosen to allow the buoyancy forces to generate the detachment of bubbles from the orifice or the injection nozzle and the slip between the liquid and gas phases. Analytical approach was first developed, then it was followed by experimental studies and more recently numerical simulation became an interesting tool for analysis of these phenomena.

Analytical models of bubble growth were developed by many authors among which Hayworth and Treybal (1950), Forster and Zuber (1954), Scriven (1959), Davidson and Schuler (1960), Rao et al. (1966), Scheele and Meister (1968, 1969), Kumar (1971),

Gaddis and Vogelpohl (1986), Oguz and Prosperetti (1993), Kim et al. (1994), Riznic et al. (1999), Chen et al. (2001), Barhate et al. (2004), Xu et al. (2005), Javadi et al. (2006), Timgren et al. (2008). The analytical models aimed at determining the evolution of the bubble size from its formation to detachment. In most of these works, the authors assumed that the bubble retains a spherical geometry. These theoretical models, based on the fundamental Newton's first law applied to the bubble entity, have limitations due to the simplifying assumptions necessary to solve these equations.

Experimental works also were carried out since the beginning of the last century. We may cite the oldest, which is the work of Harkins and Brown (1919), then those of Van Stralen et al. (1975), Peregrine et al. (1990), Shi et al. (1994), Richards et al. (1995), Wilkes et al. (1999), Notz et al. (2001), Doshi et al. (2003). More recently other works were done by authors such as Ghaemi et al. (2010), Vafaei and Wen (2010), Ma et al. (2012), Bari and Robinson. (2013), Lesage and Marios (2013), Jobehdar et al. (2016). Most of these works focused on measuring bubble volume, geometry and dynamic contact angle. The authors investigated the effect of physical properties of fluids, flow rates and the size of the orifice on the growth and detachment of bubbles. Bari and Robinson (2013a) studied the quasi-static bubble growth in water in the presence of gravity for different gas flow rates and orifice sizes. These authors showed that the size of the orifice has a significant influence on the formation of bubbles. They proposed an empirical correlation to evaluate the volume of bubbles at detachment as a function of gas velocity and the physical properties of fluids. Their results were in good agreement with those of Harkins and Brown (1919), which date back nearly a century. Bari and Robinson (2013a) observed three stages of bubble growth during its formation. A first stage, where the bubble increases in volume while maintaining a truncated spheroid type geometry. A second stage, where the bubble lengthens in the vertical direction due to increased buoyancy. This buoyancy becomes

sufficiently important to generate a third stage characterized by the formation of a neck at the base of the bubble. This elongates until it breaks to detach the bubble from the orifice. Thoroddsen et al. (2007) and Bolanos-Jimenez et al. (2016), Gordillo (2008) studied the effects of the different fluids on the dynamics and shape of the pinch-off neck of a bubble injected through a nozzle immersed in stagnant liquid. Their results show that for the largest viscosity, the contact line appears to detach from the inner corner of the needle, which may affect the overall shape and rise velocity. Vafaei and Wen (2010) investigated air bubble formation from a submerged micrometer nozzle at low air flow rates. They found that the geometric characteristics of the bubble during its growth strongly depend on its volume.

Since the 2000's, numerical studies on the formation and detachment of bubbles have become numerous. They focused on the interface capturing and tracking techniques to locate mobile interfaces separating the two immiscible fluids in order to predict the geometry of the discontinuous phase. Some works provided also an assessment of the different forces acting on the bubble during its growth. Hua and Lou (2007), Quan and Hua (2008), studied the effects of the different properties of fluids on the pinching of bubbles injected through a nozzle immersed in stagnant water. Albadawi et al. (2013b) studied the characteristics of the growth and detachment of air bubbles from a submerged orifice by comparing the experimental results with those obtained by the different interface tracking methods. These authors found that all methods give similar trends during bubble growth with significant oscillations of the bubble, which were not observed experimentally. For the same configuration, Georgoulas et al. (2015) utilized the OpenFOAM code to study the effect of physical properties of fluids and gravity on the formation of bubbles. Bari et al. (2013b) used the TransAT software to study the influence of gravity level ($0.1g < \gamma_g < 1.5g$) on the growth and detachment of bubbles from an orifice

in a liquid at rest. These authors noted that gravity has an important role on the formation of bubbles. They also showed that the volume of detached bubbles is inversely proportional to gravity and that the characteristics of the detached bubble depend on the relative influence of the pressure force and the gravity force.

Most of the works done to date in this field did not bring any particular attention to the contact line (CL) that separates the three phases, solid, liquid and gas, at the injection orifice. For most theoretical, experimental or numerical works, the authors implicitly assumed that the CL is located and pinned at the inner diameter of the injection nozzle. To our knowledge only the experimental works of Vafaei and Wen (2010), Gnyloskurenko et al. (2003), Wang (2009), Corchero et al. (2006) dealt with the motion of this CL during bubble growth. For micrometric nozzles, Vafaei and Wen (2010) showed that bubble formation goes through three stages while observing the movement of the CL. These authors observed a displacement of the CL from the inner edge to the outer edge of the nozzle wall. This line remains fixed during the elongation stage of the bubble then moves back inward until reaching the inner radius of the nozzle. Gnyloskurenko et al. (2003) and Wang (2009) considered that the bubble growth goes through 4 stages. For the case of a nozzle of millimeter diameter, Gnyloskurenko et al. (2003) found that the radius of the CL has a low dependence on the gas flow rate. For large nozzles, Corchero et al. (2006) reported a low dependence of the maximum radius of the CL on flow rates for equilibrium contact angles greater than 90°.

From this literature review, several comments may be made. First, the main configuration considered is a vertical injection of the gas through an orifice or an injection nozzle in a stagnant liquid. Then, during nearly a century, a great deal of analytical and experimental work was conducted on the formation and detachment of bubbles. Whereas, numerical studies on this topic are more recent and have become more important over the past two

decades. Many studies aimed at analyzing the influence of the physical properties of fluids, the respective flow rates of the phases, the diameter of the injection nozzle on the formation of bubbles and their sizes at detachment. More recent work has investigated the influence of gravity magnitude on bubble formation (Bari et al. (2013b), Das and Das (2015), Nahra and Kamotani (2003), Georgoulas et al. (2015)). Regarding the results, the majority of studies focused on the prediction of bubble volume during the growth and at detachment by applying a force balance on the bubble. In this context the authors Vazquez et al. (2010), Bari et al. (2013b), Bari and Robinson (2013a), Albadawi et al. (2013a), Vafaei and Wen (2010)), showed that the gravity force has a great influence on the detachment of the bubble.

Overall, the numerous studies conducted nearly for a century allowed a better understanding of the mechanism of bubble formation at orifices or nozzles immersed in a liquid for given orientations of the injection with regard to gravity. However, the recent work done over the last few years showed the need to further explore this topic as many questions remain open, in particular about the mechanisms of bubble formation in the absence of gravity.

The other issue very little investigated concerns the formation of bubbles from micro-orifices. Achieving experiments at these scales still presents many challenges and both experimental and numerical studies are very limited (Vafaei and Wen (2010), Bari and Robinson (2013)). Experimentally, the main reasons lie in the difficulty of implementing accurate investigation techniques for these small dimensions (Zeguai et al. (2013)). Numerical difficulties are mainly related to the treatment of mobile interfaces under conditions of two-phase flow in confined spaces. Moreover, the mechanism of bubble formation and detachment requires an exploration of the phenomena at scales smaller

than those explored to date, particularly at the contact line, which has received very little attention.

The present study is carried out in this context by addressing these issues. It aims at analyzing numerically bubble growth and detachment emerging from a micro-tube in a liquid flow under two different levels of gravity (0 and 1 g).

In the next section, we present the physical model and the mathematical formulation to predict the two-phase flow in the entrance zone where the two phases are brought in contact. The volume of fluid (VOF) method is implemented to track and locate the interface and its induced deformations. It is followed by the section dedicated to the numerical tool used i.e. the open source code OpenFOAM (Open Field Operation And Manipulation). The bubbly flow regime is considered with laminar flow conditions to yield smooth interfaces and analyze the bubble growth and detachment. Then, the prediction results are presented in the next section. It is organized such as a qualitative description, which is first given through numerical visualizations and the geometrical characteristics of the bubble with a focus on the contact line motion along the injector wall, is presented. It is followed by a quantitative assessment of the forces acting on the bubble for an upward flow with gravity contribution. The magnitude and the role of the surface tension force is highlighted during attachment and pinching of the bubble. The paper is ended with a conclusion on the mechanisms of formation and detachment of bubbles in a co-flowing water-air flow and highlighting the dynamics of the associated contact line at the injector wall.

2. Mathematical Formulation

The mathematical formulation relies on a physical model that consists of a micro-tube of 500 μm inner diameter carrying water flow in which air is injected axially through a centered nozzle of 110 μm inner diameter and 210 μm outer diameter (Fig.1).

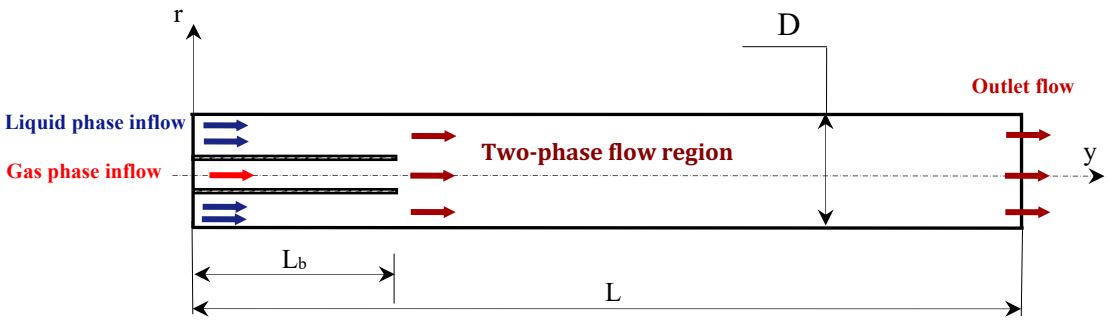

Figure 1: Schematic representation of the physical and computational domain. At the inlet, the gas phase flows inside the nozzle and the liquid flows at the outside of the nozzle. The two-phase flow is generated at the nozzle exit ($y=L_b$)

Each fluid flows under laminar flow conditions in order to deal with smooth interfaces. To predict the liquid and gas flows in the micro-tube, the mass balance and momentum equations of each of the phases with the associated boundary conditions are solved numerically.

The flow is assumed adiabatic and axisymmetric. The two immiscible fluids have uniform inlet velocities that allow laminar flow conditions and meet at the exit of the nozzle to yield a two-phase flow (Fig.1). In the present study, both fluids are considered incompressible and Newtonian. The flow field is governed by the conservation equations (mass and momentum) and the volume of fluid method is utilized to locate the interface between the liquid and gas phases. In this method, as it was proposed by Hirt and Nichols (1981), the flow equations are volume averaged directly to obtain single set of equations and the interface is tracked using a phase indicator function φ (also known as color

function or volume fraction). This discrete function φ takes values between 0 and 1. The limiting values of 0 and 1 mean that only one phase is present; intermediate values mean that a two-phase mixture exists and the interface is present (Gopala and Wachem(2008)). The mass and momentum equations can be written as:

$$\frac{\partial}{\partial t}(\rho\vec{u}) + \nabla.(\rho\vec{u}) = 0 \quad (1)$$

$$\frac{\partial}{\partial t}(\rho\vec{u}) + \nabla.(\rho\vec{u}\,\vec{u}) = \nabla.\vec{T} + \rho\,\vec{g} + \overrightarrow{F_s} \quad (2)$$

Where ρ is the density of the fluid, u is the velocity vector; t is the time, T the stress tensor and g the gravity vector. F_s is the tension force per unit volume acting on the interface between the two fluids and calculated by the Continuum Surface Force (CSF) model.

Where T is the stress tensor defined as:

$$T = P + \nabla(\mu\, u) \quad (3)$$

The density ρ and viscosity μ are computed as the averages over the two phases, weighted with the volume fraction φ

$$\rho = \varphi\rho_1 + (1-\varphi)\rho_2 \quad (4)$$

$$\mu = \varphi\mu_1 + (1-\varphi)\mu_2 \quad (5)$$

The surface tension force F_s is modeled as in Brackbill et al. (1992), applying the following equation:

$$\overrightarrow{F_s} = \sigma\,\kappa\,\vec{n} \quad (6)$$

Where σ is the surface tension, κ the curvature of the interface and $\vec{n}$ the outward unit vector normal to the interface.

The curvature of the mobile interface is computed as:

$$\kappa = \nabla.\vec{n} \quad (7)$$

The unit vector n is given by the following equation:

$$\vec{n} = \frac{\nabla.\varphi}{|\nabla.\varphi|} \quad (8)$$

The scalar φ being the volume fraction. Its evolution is governed by the advection equation:

$$\frac{\partial}{\partial t}(\varphi) + \frac{\partial}{\partial x_i}(u_i\,\varphi) = 0 \quad (3)$$

3. Numerical Method

3.1. Numerical Domain and Mesh

An axisymmetric computational domain, encompassing hexahedral and prismatic elements, is constructed and a hybrid computational mesh is used with different levels of refinement. Mesh dependency study is conducted, showing the numerical solution is mesh-independent for a spatial step size of 1μm. Figure3 illustrates the mesh and boundary conditions, as well as the computational domain constructed which consists of a wedge type geometry representing a 5 degrees section of the corresponding 3D domain of the considered physical problem (Greenshields (2015)).

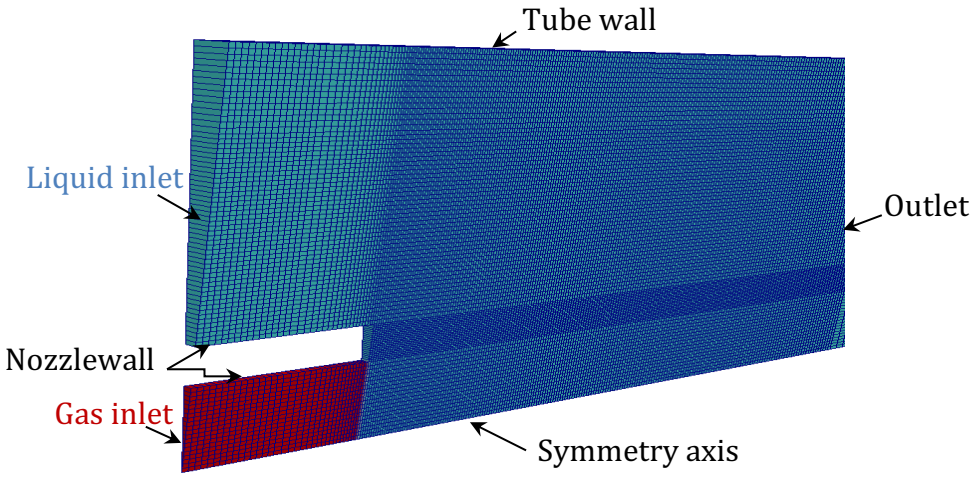

Figure 3: Computational domain, mesh.

A no-slip velocity boundary condition was used for the walls. At inlets, constant volume fraction values and uniform inflow velocity profiles for the gas phase and for the liquid phase are applied. For the outflow boundary, we applied a given value for the pressure and a zero-gradient for the velocity and for the volume fraction.

Eventhough the equilibrium contact angle between the wall and water depends on the water purity and on the surface roughness and wettability. Gerlach et al. (2007) showed that if the contact angle, imposed in a numerical simulation, is below a limiting value, the contact line stays pinned at the orifice. Georgoulas et al. (2015) reported on this contact angle value to be of 20°.

In the present work, two situations were investigated. The first one corresponds to a moving contact line in order to look at its effect on bubble formation and detachment. The second corresponds to fixed contact line. Gerlach et al. (2007) found that the contact line remains fixed to the inside radius of the nozzle when the contact angle is less or equal to 20°. This result was applied by several authors like Georgoulas et al. (2015) and Albadawi

et al. (2013b). Whereas, other authors like Vafaei et Wen (2010), Gnyloskurenko et al. (2003), Wang (2009), Corchero et al. (2006)) considered in their experimental works that the contact line may be moving. It has been found that the radius of the contact line ranges between the inner and the outer radius of the nozzle. This point will be discussed in detail in results section.

3.2. Solution Method

An open source code, OpenFOAM (Open Field Operation And Manipulation), based on the control volume method is used to solve the governing equations.

The standard form of the transport equation for a scalar property ϕ is:

$$\underbrace{\frac{\partial}{\partial t}(\rho\Phi)}_{\text{transient term}} + \underbrace{\nabla.(\rho\, u\, \Phi)}_{\text{convection term}} + \underbrace{\nabla.(\Gamma_{\Phi}\, \Phi)}_{\text{diffusion term}} = \underbrace{S_{\Phi}(\Phi)}_{\text{source term}} \quad (10)$$

where ρ is the density, u the velocity field and Γ the diffusion coefficient.

Standard discretization schemes are applied within the control volume approach. The transient terms in the equations are discretized using a first order implicit scheme (Euler) with Courant number (CFL) smaller than 0.5.The convection term in the momentum equation is discretized using a Gauss limited linear scheme. The convection term in the VOF equation is discretized using the Gauss vanLeer scheme. Finally, diffusion term is discretized using the Gauss Linear Corrected scheme (C.J. Greenshields (2015)).

The adopted solution method for the resulting algebraic equations is the preconditioning gradient method (PCG) with diagonal incomplete-Cholesky preconditioner for pressure and bi-conjugate gradient (PBiCG) with diagonal incomplete-LU preconditioner for velocity. In the interFoam solver available in OpenFOAM Code, the pressure-velocity coupling is handled with PISO (Pressure Implicit with Splitting of Operators) algorithm (Issa 1986; Schulze 2014).

The convergence criterion of the computation iterative process is achieved for each time step when the residuals of pressure and velocities are less than 10^{-6}.

Appropriate mesh refinement has been implemented in InterFOAM, the solver of OpenFOAM, in order to capture and locate the interface with VOF method with clearness and obtain a smooth interface.

3.3. Validation

Before running our cases, we have checked the computer program by comparing obtained results with published ones in the literature. Several comparisons have been made with results of Georgoulas et al. (2015), Bari et al. (2013) and Quan and Hua (2008) and a good concordance was found. In this work, we present only results related to bubble formation and the comparison with the experimental and numerical results of Quan and Hua (2008). The comparison is conducted for the same conditions as the experimental and numerical work of Quan and Hua (2008) for neck formation and bubble detachment i.e. R_b= 1.35 x 10^3µm, ρ_g= 1.005 kg/m^3, ρ_l= 10^3 kg/m^3, μ_g=0.0142 mPa·s, μ_l=1.48 mPa.s, σ=0.065 N/mand g=9.81 m/s^2.Figure 4 illustrates the comparison for the pinching of an air bubble emerging vertically from a 1.35 mm radius nozzle immersed in water at rest. A very good agreement is observed with our results. Therefore, it can be concluded that the computational code reproduces fairly the phenomena of bubble formation and detachment, and it allows to conduct safely numerical experiments aimed at understanding this type of phenomena. Other comparisons have been performed with further experimental results. These will be presented later in the results section.

a)

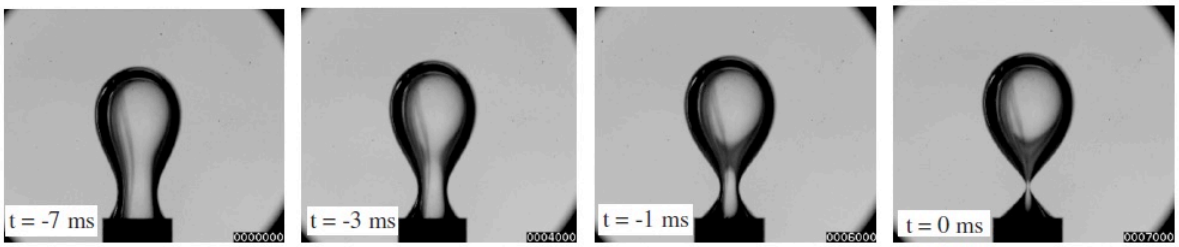

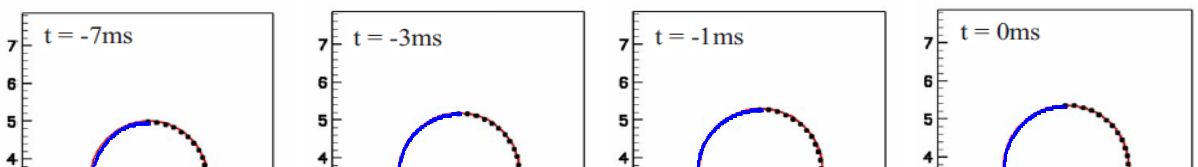

b)

a)

Figure 4: a) Snapshots of the experimentally observed air bubble pinch-off process in water by (Quan and Hua, 2008), b) comparison of the bubble shapes predicted by simulation (dotted black line) and observed in experiments (solid red line) (Quan and Hua, 2008) with numerical present study (blue plus line) before the time of detachment (t = 0 s).

4. Results and discussion

Results are obtained for a co-current flow in a tube of 500 μm inner diameter with an injection nozzle of 110 μm inner diameter and 210 μm outer diameter. It carries the gas phase on a length of $30x10^3$ μm before it mixes with the liquid phase (Fig. 1).

4.1. Numerical Visualization

Based on the visualization of a bubble starting from its formation at the exit of the injection nozzle to detachment, Figure 5 illustrates the phase function φ which shows two different colors, the red color represents the liquid phase and the blue color represents the gas phase. The gas flow rate at the inlet of the pipe is 2.85×10^{-9} m^3/s and that of the liquid is 1.29×10^{-8} m^3/s corresponding to superficial gas velocity of 14.52×10^{-3} m/s and superficial liquid velocity of 76.12×10^{-3} m/s for a horizontal orientation of the tube. From Fig.5, we see that the formation of the bubble undergoes three stages, the first stage represents the bubble growth, while the second represents the elongation of the bubble. The last stage represents the formation of the neck followed by the pinch-off and the detachment of the bubble. During the first stage i.e. expansion stage (Fig. 5a), the bubble

grows with time due to continuous injection of gas through the nozzle. The bubble always remains attached to the nozzle under the effect of the surface tension force and rapidly increases in volume in both directions of the pipe (radial and axial) which gives it a hemispherical shape. The second stage, i.e. elongation stage (Fig. 5b), begins when the bubble becomes large enough and it begins to stretch in the direction of flow and to have a length greater than its radius. The last stage, called the pinch-off stage (Fig. 5c), starts when the bubble is stretched to a certain length, as the elongated bubble loses its stability, it narrows inwards creating a pinch near its base and distant from the nozzle forming a neck. The diameter of the latter decreases with time until it induces the detachment of the bubble at this position.

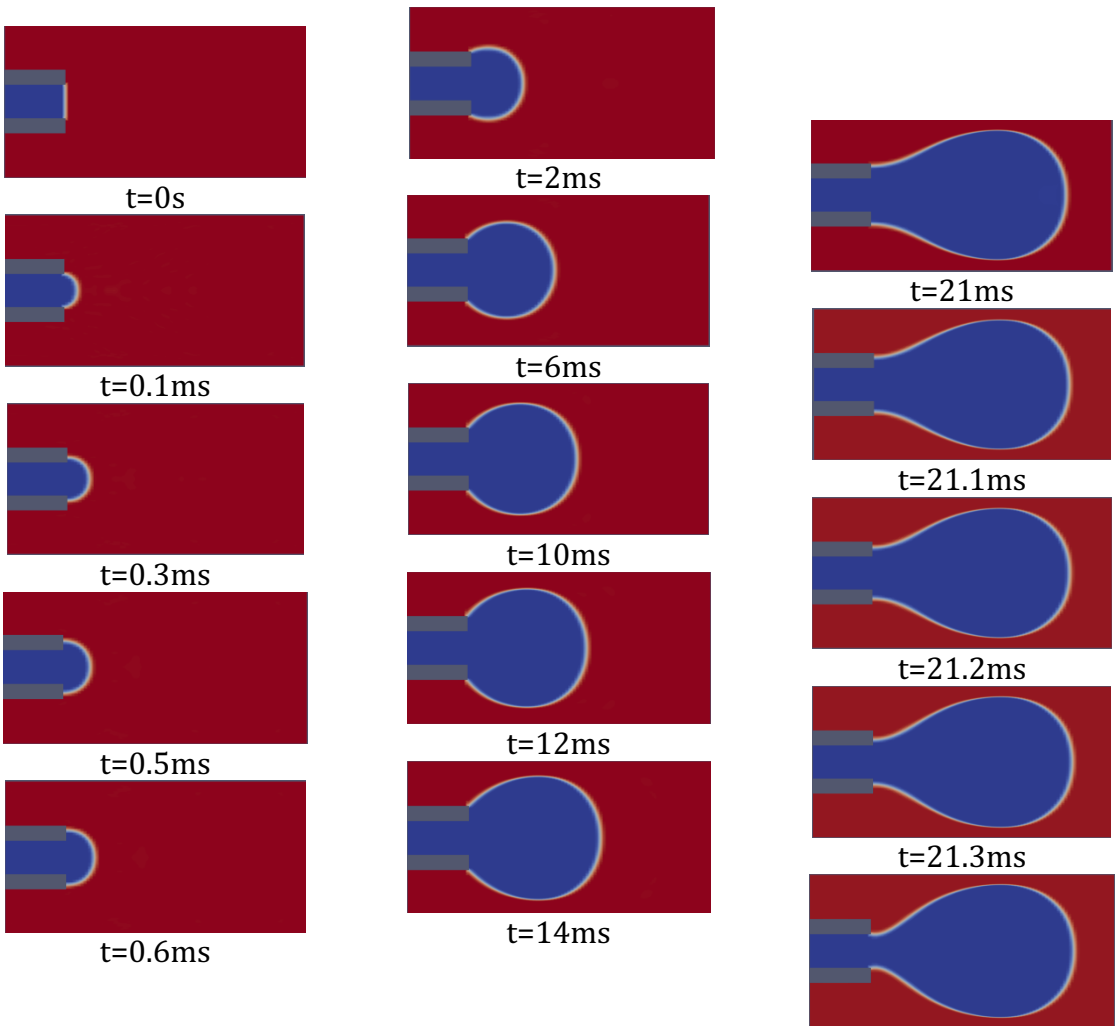

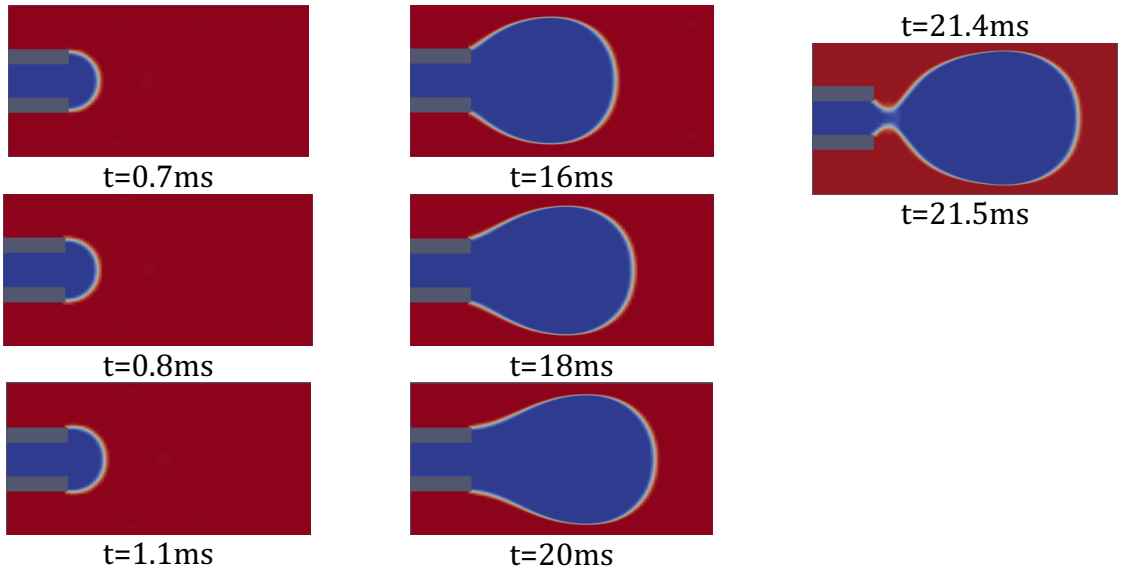

a) Stage1: Bubble growth (0 ms < t < 1.1 ms)

b) Stage 2 : Bubble stretching (1.1 ms < t < 20 ms)

c) Stage 3: Neck formation and bubble detachment (20 ms < t < 21.5 ms)

Figure 5: Visualization of bubble formation and detachment (U_{GS}=0.014 m/s, U_{LS}=0.076 m/s).

Indeed, this phenomenon is only a consequence of the effects of the surface tension force on the bubble, which keeps the bubble attached to the wall in the first and the second stage, whereas it contributes to the formation of the neck and the detachment of the bubble in the last stage.

4.2. Bubble shape evolution and contact line motion

Figure 6 represents the quantitative evolution of the bubble as a function of time for a horizontal pipe. The continuous injection of the gas induces the increase of the bubble volume which generates a pressure difference between the inside and the outside of the bubble. Surface effects give rise to mobile interfaces that significantly affect the shape of the bubble as a function of time.

We observe several stages characterized by different bubble shapes such as those shown in Figs. 6a, 6b, 6c.This figure also shows that the contact line is mobile as a function of time

for the first and the last stage of bubble formation (Figs. 6a and 6c). During the first stage, the contact line moves outward and its radius increases from the inner radius to the outer radius of the nozzle. Then, during the second stage, the contact line remains pinned at the outer edge of the nozzle wall, while the bubble continues to grow and stretches (Fig. 6b). In the last stage, the contact line moves back and its radius decreases to the inner radius of the nozzle. It is followed by the neck formation (Fig. 6c), which is characterized by the reversal of the curvature of the interface. From these figures, the three stages of bubble formation that have been proposed in the qualitative visualization (Fig.5) have been confirmed and classified according to the shape of the bubble and the displacement of the contact line.

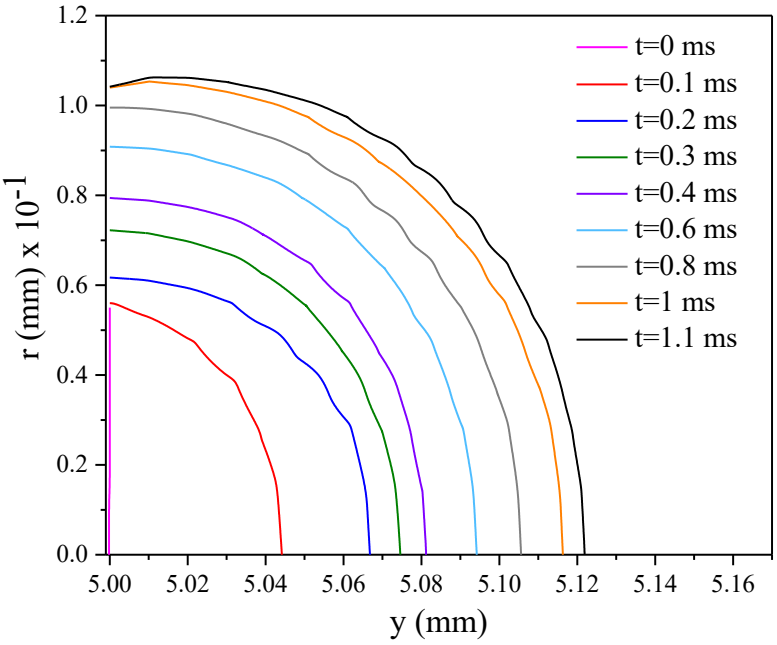

a) Stage 1 : Bubble growth and increasing contact line radius ($0 < t < 1.1$ ms)

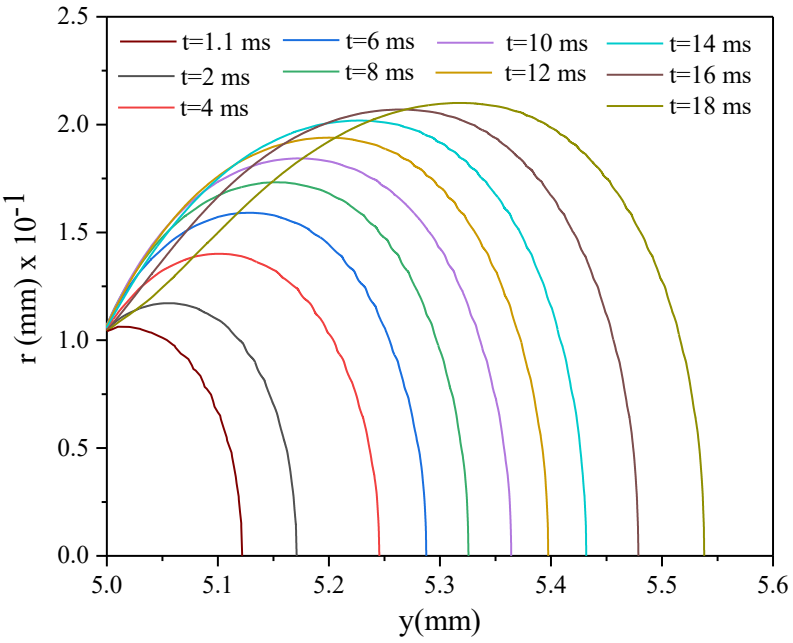

b) Stage 2 : Bubble stretching and pinned contact line (1.1 ms< t <20ms)

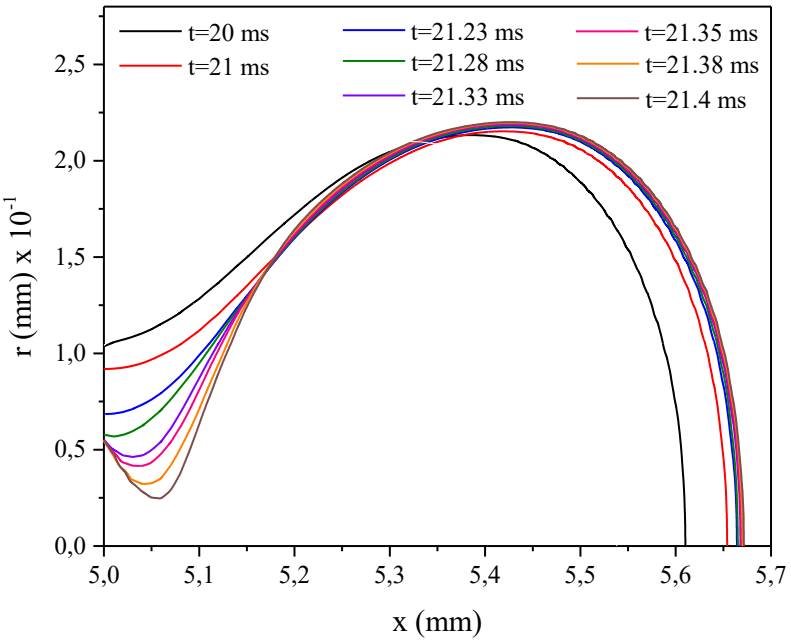

Stage 3: Decreasing contact line radius till to the inlet nozzle diameter and neck formation with its evolution over time (20ms< t < 21.5 ms)

Figure 6: Bubble shape evolution and contact line motion (U_{GS}=0.014 m/s, U_{LS}=0.076 m/s).

With the condition of no slip velocity at the walls of the gas injection nozzle and without setting the static contact angle at t = 0 s, we obtain a movable contact line. Indeed, to confirm this result which is illustrated in Fig. 6, we have plotted the evolution of the radius of the contact line R_0 as a function of time (Fig. 7). This figure shows that the formation of the bubble is characterized by three stages highlighted by visualization (Fig. 5) and shape and size (Fig. 6). The first step occurs at the beginning of the bubble formation when the time is less than a critical value t = 1.1 ms; in this step the contact line radius increases rapidly and reaches the outer radius in a few milliseconds. The growth of the bubble and its stretching continue in the second stage, where the contact line is pinned at the outer radius of the nozzle. This stage lasts the majority of the bubble formation period and goes up to the instant t = 20 ms. In the last step at the end of bubble formation, the radius of the contact line decreases rapidly until it reaches the inner radius of the nozzle. At this moment the neck is formed and its diameter decreases rapidly to a null value which gives rise the bubble detachment.

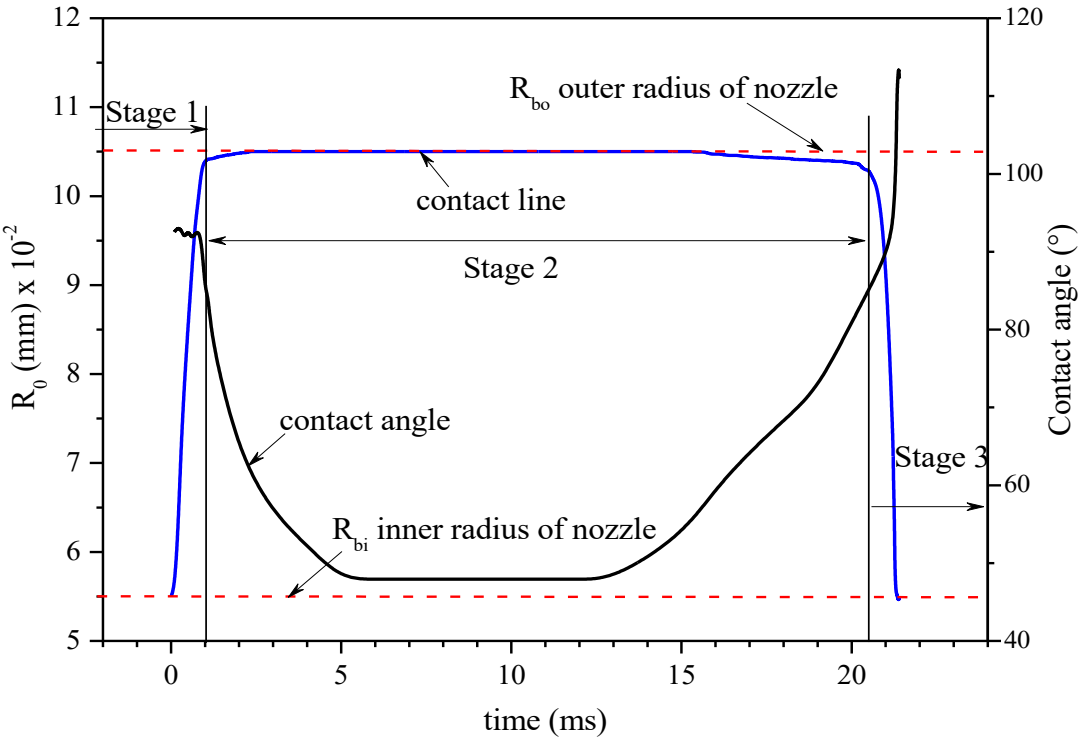

Figure 7: variation of contact line radius and the contact angle versus time. The three stages are clearly highlighted for the contact line radius (U_{GS}=0.014 m/s, U_{LS}=0.076 m/s).

As mentioned previously, the contact angle is not set at a prescribed value, but varies instantaneously. It is defined as the angle between the tangent to the interface of the bubble and the wall and is measured in the liquid phase. Figure 7 displays also, on the right axis, the variation of the instantaneous contact angle as a function of time. It exhibits a plateau at the beginning of the formation of the bubble followed by a U shape. This plateau indicates that the instantaneous contact angle is constant for a very short period (0 < t <1 ms), which corresponds to the rapid displacement of the contact line (Figs. 6a and 7. The trend of this profile changes from the instant t = 1.1 ms. Indeed, a rapid decrease as a function of time is observed as the bubble deforms; then another plateau is displayed, which means that the contact angle is constant during the period 5 < t <14 ms, corresponding to the stage of bubble stretching during which the contact line is pinned

(Fig. 6b and 7). Then, the contact angle increases again with the return of the contact line to its initial position, which corresponds to a contact angle equal to 90 °. Whereas, the last stage of detachment is characterized by the increase of the contact angle Θ> 90 ° due to the formation of the neck (Fig. 6c).The wettability conditions are generally defined according to the contact angle. If these conditions are projected on the variation of the dynamic contact angle (Fig.7), it is found that at the beginning of the bubble formation, the contact angle Θ is close to 90 °, the wettability of the fluid is neutral. Then, the contact angle decreases to an optimal value and during this period the liquid wets the nozzle wall (Θ<90°). And from this minimum, the contact angle increases until the detachment. It goes through two steps, the first where Θ < 90 ° and the second step where Θ > 90° which gives less wetting walls. In this step there is a creation of the neck followed by the detachment of the bubble. The analysis of the previous figures helps understanding the dynamics of the contact line and looking for the dominant parameters of this phenomenon as well as their influence on bubble formation.

A literature survey showed that studies that considered the contact line motion are rather rare. Vafaei and Wen (2010) reported on the motion of the contact line at the air injection orifice to analyze bubble formation emerging from a nozzle which was immersed in stagnant water. As previously mentioned, we carried out a comparison with the work of Vafaei and Wen (2010) under the same conditions i.e. for the case of an air flow rate of 0.83 ml/min (1.38×10^{-8} m^3/s) and a nozzle whose inner and outer radius are 0.11mm and 0.21mm respectively. Our numerical results as compared with the experimental ones of these authors for the same conditions showed a good concordance as illustrated in Fig.8.

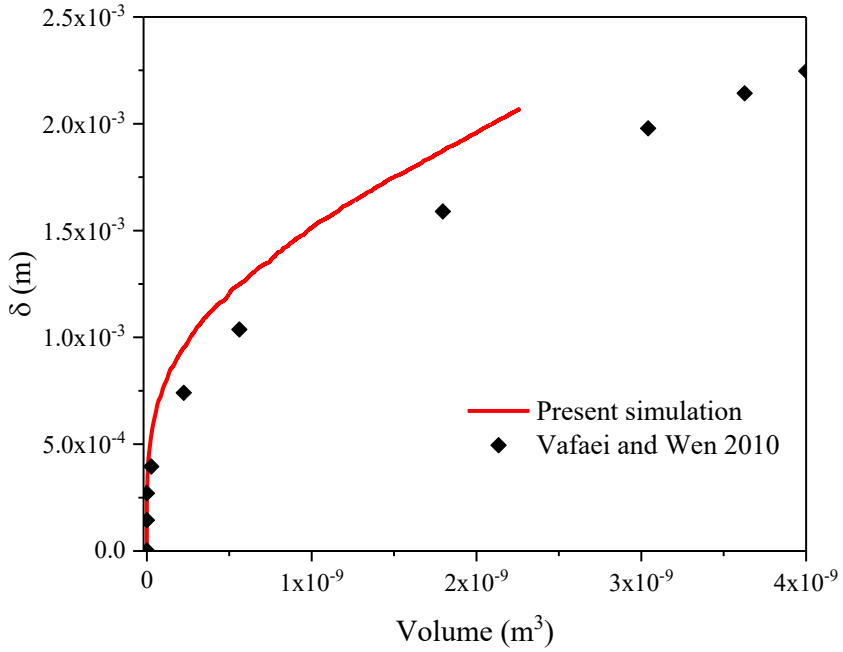

a)

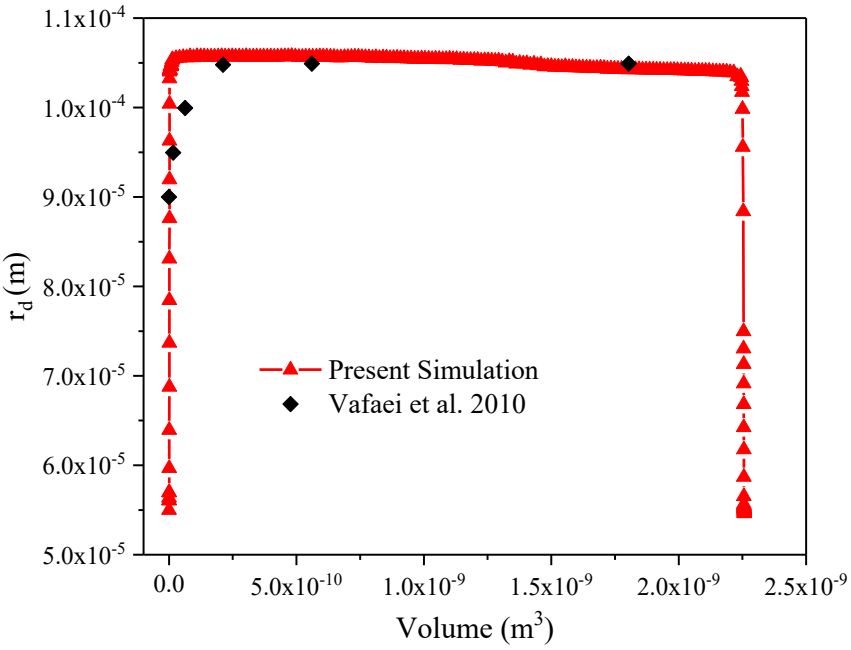

b)

Figure 8: Variation of (a) bubble length, (b) contact line radius versus bubble volume Experimental results of Vafaei and Wen and present numerical results are carried out for Q_G=0.83 ml/min (1.38 x 10^{-8} m^3/s).

Figure 8a show the variation of the bubble length as a function of the bubble volume and Fig. 8b represents the variation of the contact line radius versus the bubble volume. The length of the bubble increases rapidly at the first stage of the formation and maintains a subsequent steady increase during the second and third stages.

Numerical and experimental profile in the Figures 8a show identical variation laws, but the bubble sizes at the detachment are different. This is probably due to the kinetics of narrowing of the neck (3rd stage, Fig. 8b).This kinetics is extremely fast and it is difficult in this case to capture it experimentally with a good precision. Indeed, the duration between the beginning of the neck formation and the detachment of the bubble is a few microseconds (Fig. 8b). This third stage of bubble formation is very rapid and has not been observed experimentally by Vafaei and Wen (2010). In fact, the distinction between the different points in this stage requires extremely fast viewing means and typically camera capable of tracking millions of images per second.

4.3. Bubble detachment process

Let us focus on the end of the last stage i.e. on the bubble detachment process. Figure 9 displays the contact line radius and the neck radius during the last period of the process from 21 ms to the bubble detachment. The red curve represents the radius of the contact line and the blue curve the radius of the neck. The detachment of the bubble is characterized by very rapid change in the shape of the bubble as the neck is formed. This

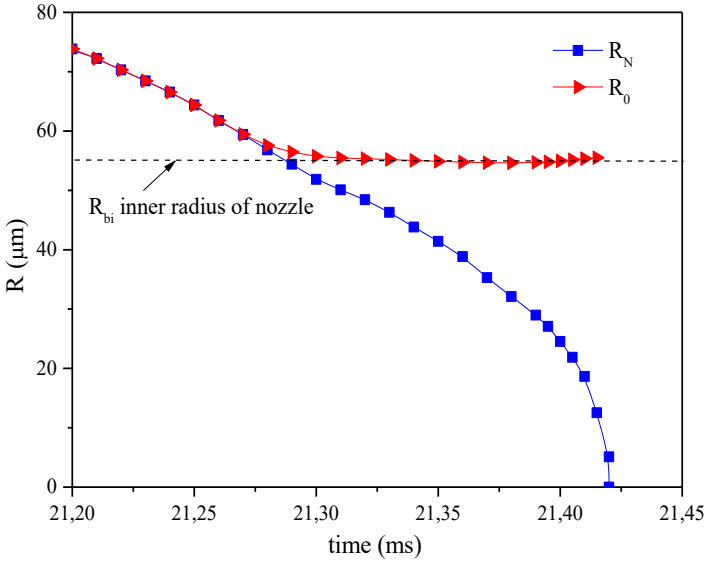

Figure 9: Variation of the contact line radius and bubble neck radiusversus time in the last instants before bubble detachment (U_{GS}=0.014 m/s, U_{LS}=0.076 m/s).

figure reveals that the formation of the neck begins when the contact line leaves the outer radius and then settles on the inner radius of the nozzle. This figure shows a rapid decrease of the radius of the neck until detachment of the bubble. In this figure, it can be noted that the narrowing of the neck evolves slowly until t =21.40 ms. Then, it sharply decreases to pinch the bubble at detachment. In the process of neck formation, the pressure in the gas phase becomes less important yielding a deformation of the bubble interface due to the capillary pressure. The effect of the surface tension force thus accelerates the pinching and the detachment of the bubble.

Furthermore, if we track the axial location of the neck, we observe a linear increase of its position with time before a rapid acceleration to produce the detachment in a few microseconds (0.01ms).It is noticed that the detachment of the bubble does not occur at the exit of the nozzle, but in its immediate vicinity at a distance of about 0.5 times the diameter of the nozzle.

4.4. Analysis of forces applied on the bubble during its formation in an upward flow.

The previous analysis related to the visualization, the shape and the size of the bubble remains a rather qualitative analysis and does not allow to fully understand the causes

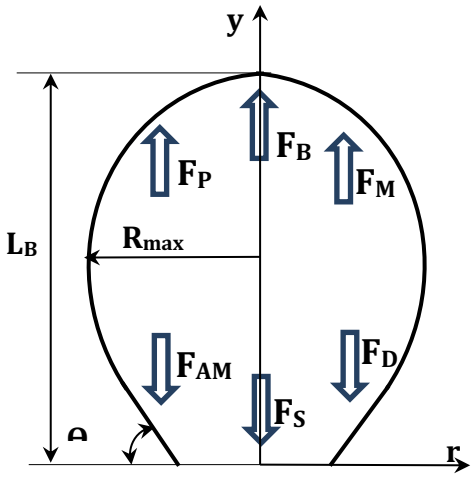

Figure 10: Schematic showing the vertical forces on a bubble during its formation

Figure 10 shows the vertical forces acting on the bubble. Two types of forces may be distinguished, the ones having an attachment role (F_{AM}, F_S, F_D) and the ones acting to detach the bubble (F_P, F_B, F_M). These forces are defined as follows:

The buoyancy force (F_B) is (as in Teresaka and Tsuge, (1993)):

$$F_B = (\rho_L - \rho_G)\, g\, V_B \tag{11}$$

where V_B is the bubble volume.

The gas momentum force (F_M) results from gas momentum through the orifice and is (as in Martin etal., (2006)):

$$F_M = \frac{\rho_G}{\pi\, r_0^2}\left(\frac{d\, Y_{CM}}{dt}\right)^2 \tag{12}$$

The surface tension force (F_S) is (as in Duhar and Colin, (2006)):

$$F_S = 2\,\pi\, r_0 \sigma \sin\theta \tag{13}$$

The viscous drag force (F_D) prior to detachment primarily is determined by growth of bubble's vertical mass centroid (dY_{CM}/dt) (as in Zhang and Shoji, (2001)):

$$F_D = \frac{1}{2}\,\pi\,\rho_L C_D r_B^2 \left(\frac{d\,Y_{CM}}{dt}\right)^2 \tag{14}$$

where C_D is the drag coefficient given as a function of Reynolds number (Re) (see Nahra and Kamotani, (2003)).

$$C_D = \frac{15.34}{Re} + \frac{2.163}{Re^{0.6}} \tag{15}$$

$$Re = \frac{\rho_L U_G d_{bi}}{\mu_L} \tag{16}$$

The added mass force (F_{AM}) arises from bubble growth and the resultant displacement of the surrounding fluid. Thus, F_{AM} is the liquid's resistance to bubble interface changes; it is given as in Li et al., (2002).

$$F_{AM} = -\frac{d}{dt}\left[\left(\rho_G - \frac{11}{16}\rho_L\right) V_B \frac{d\,Y_{CM}}{dt}\right] \tag{17}$$

The pressure force (F_P) is

$$F_P = (P_G - P_L)\,\pi\,r_0^2 \tag{18}$$

P_G and P_L being the pressure in the gas and in the liquid respectively.

At each time step, the solver of OpenFOAM supplies the data for velocity, pressure and volume fraction. A computer program is then written in C++ to compute the geometrical parameters of the bubble, its volume, its surface and all forces exerted on the bubble.

Figure 11 shows the evolution of the forces acting on the bubble as a function of time that control the formation process. The forces acting on the bubble are divided into two main groups according to their influence on the formation (Duhar and Colin, 2006, Bari and

Robinson, 2012). The first group promotes the detachment of the bubble and includes the buoyancy force and the pressure force, the other group of forces resists the detachment of bubbles and acts to maintain the bubble attached to the orifice as the surface tension force.

Under quasi-static conditions only gravity force, pressure force, surface tension force as well as the resultant of all the forces mentioned above are shown on this figure. The other forces remain negligible.

From this figure, we notice the three stages during bubble formation as reported previously. Let's recall that the negative forces are playing an attachment role and the positive forces a detaching role. For the first stage, the magnitude of the surface tension force increases to a maximum value as well as does the pressure force. However, the magnitude of the surface tension force is always greater. Indeed, the displacement of the contact line induces the increase of the surface tension force in order to maintain the bubble attached to the nozzle. The dominance of this force, which is an attaching force, does not allow detachment by other forces applied on the bubble. In this step, the dynamic contact angle is almost constant and therefore has no influence on the bubble formation and the forces applied on it. However, the displacement of the contact line has a remarkable influence on the forces applied on the bubble and on its formation. Moreover, the optimum of the forces which limits this stage corresponds to the upper limit of the contact line radius which equals the outer radius of the nozzle (Fig. 7).

For the second stage, the magnitude of the surface tension force decreases and then it remains relatively constant while the contact line is pinned to the outside radius of the nozzle. Therefore, the behavior of the surface tension force is rather influenced by the instantaneous contact angle (Fig. 7). The decrease of the pressure force during this

formation step is explained by the pressure difference between the two phases because the radius of the contact line is fixed.

During the third stage, a decrease of the magnitude of the surface tension force is observed and at the end of the process a sharp drop of the surface tension force yields the pinch-off and detachment of the bubble.

The trend of the pressure force shows a rapid decrease with the return of the contact line to its initial position at the inner radius of the nozzle. This coincides with the beginning of the neck formation and the reversal of the curvature of the interface. However, the surface tension force decreases mainly because of the inward motion of

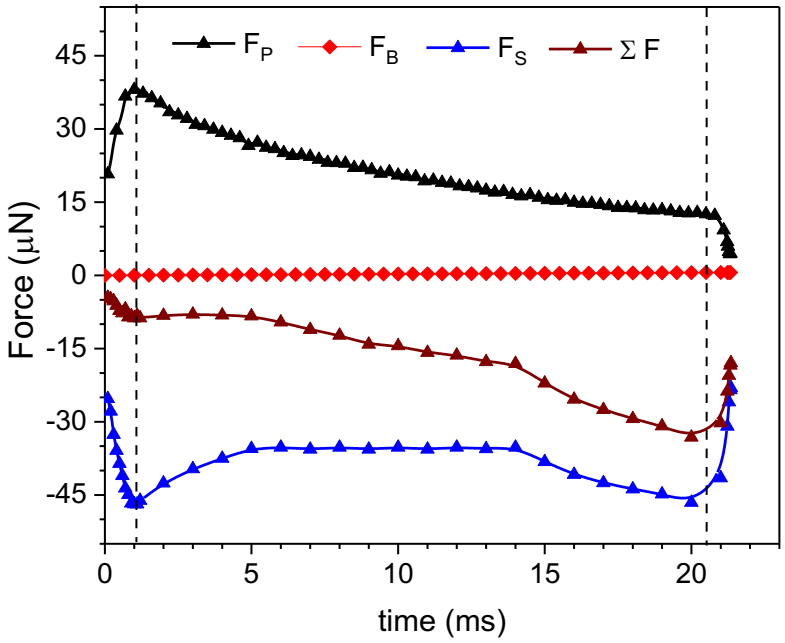

Figure 11: Evolution of vertical forces acting on the bubble

the contact line and the decrease of its radius as well as the increase of the angle of contact over 90°. On the other hand, we may highlight that although the tube is vertical and we consider an upward flow, the gravity force is not playing any significant role in this

context of small size bubbles. The gravity force very slightly increases linearly with time (up to 0.6 μN), but remains negligible compared to other forces.

After reviewing the possible mechanisms of bubble formation for very low Reynolds number, we thought that the mechanism of bubble detachment may be caused by surface tension force under these conditions. Contrary to the conventional mechanistic approach where the surface tension has a role of attachment to the injection nozzle, in this case, the surface tension may play a double role, it causes the attachment of the bubble to the nozzle during the first 2 stages and then it contributes to destabilize the interface during the last stage, by creating the neck which is followed by the pinch-off and detachment of the bubble. From the birth of the bubble at the injection nozzle with the shape of a spherical cap, it increases in volume while the contact line moves outwards. Then, it keeps increasing in volume and stretching while the contact line is pinned at the outer nozzle radius and a cylindrical neck is formed. It is followed by an inward motion of the contact line to its initial position and then the destabilization effect of the surface tension force starts and generates a minimal surface feature illustrated by the narrowing of the neck. This amplifies until the pinch-off and the detachment of the bubble of a spherical shape. This description is verified by the evaluation of the surface/volume ratio of the bubble from its birth to breakup (Fig. 12). This figure shows a continuous decay of this specific surface from the formation of the bubble at the injection nozzle to detachment at the neck.

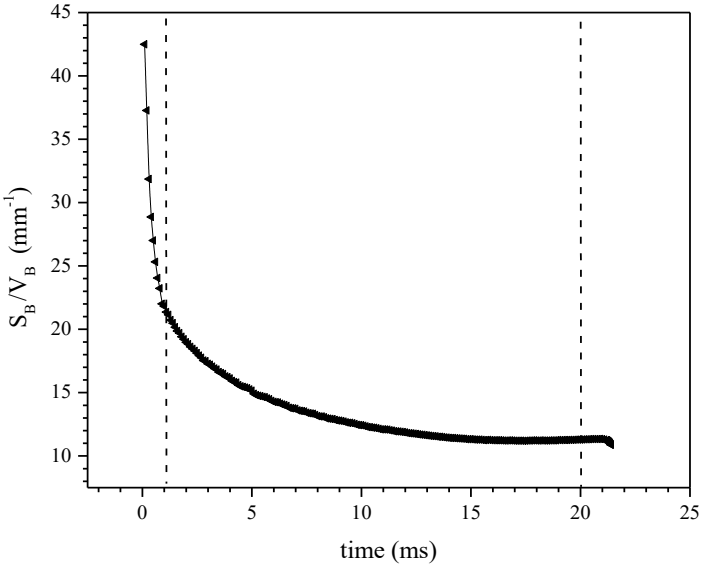

Figure 12: Bubble Surface/Volume ratio versus time
(U_{GS}=0.014 ms U_{LS}=0.076 m/s).

4.5. Effect of the contact line motion

In order to highlight the influence of the contact line motion on forces applied on the bubble, we have considered the cases of a free contact line and a fixed contact line at the injection nozzle (Fig. 13). The case of Fig.13b refers to a contact line pinned at the inner nozzle radius as done in most reported works in the literature. It is clear that the contact line radius impacts directly the forces exerted on the bubble and particularly the surface tension force and for instance has a significant effect on bubble formation, detachment time and bubble size. It is shown that the assumption of a fixed contact line reduces substantially the magnitude of the surface tension force and does not show the first stage of the bubble formation as described previously. Moreover, the difference lies in the detachment time, the detached bubble volume and the forces applied on the bubble. Indeed, the detachment time by fixing the contact line is reduced by over 30 % as compared to that of a moving contact line. The volume of the detached bubble produced

with a moving contact line is nearly 1.5 the bubble volume detached when assuming a pinned contact line. In addition, a remarkable difference between the pressure forces is exhibited for both cases. The pressure force with a movable contact line is greater than that with a fixed contact line i.e. the pressure inside the bubble for the first case is greater than that of the second case. Nevertheless, the strength of the surface tension force is dominant in both cases and the gravity force is negligible.

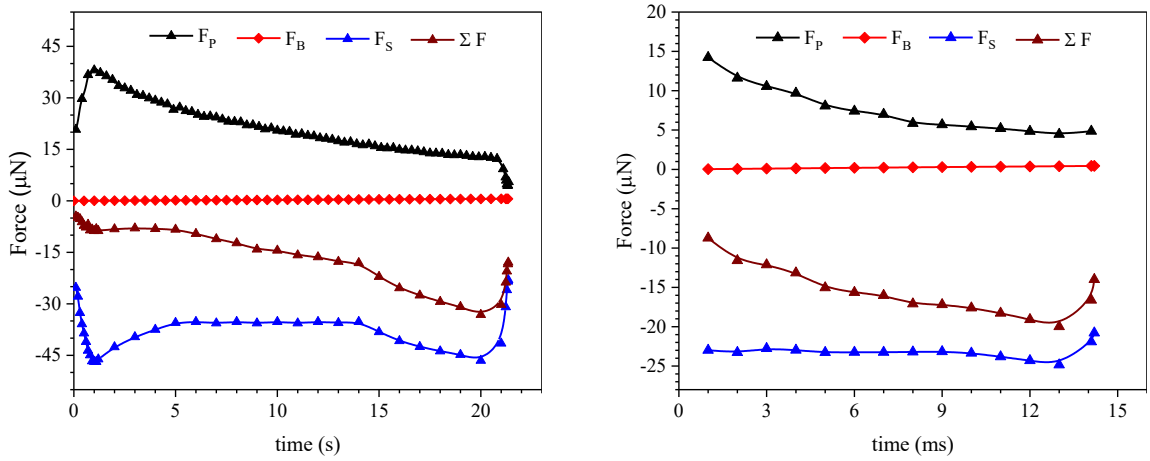

a) Mobile contact line b) Fixed contact line

Figure 13: Effect of contact line motion on forces exerted on the bubble

5. Conclusion

The study of bubble growth and detachment in a co-flowing two-phase flow in a cylindrical micro-tube is carried out to analyze the role of surface tension force with or without gravity. Two configurations are considered, a horizontal axisymmetric flow in the absence of gravity and an upward flow in the presence of gravity. The open source code "OpenFOAM" is implemented to simulate the mechanism of growth and detachment of bubbles for a two-phase air-water flow in a micro-tube using the Volume of Fluid method for tracking the mobile interface.

The prediction results show that the bubble detachment does not occur at the exit of the nozzle, but in the immediate vicinity of the nozzle at a distance of about 0.5 times the nozzle diameter.For very small nozzles, the diameter of the bubble is smaller than the capillary length (capillary regime), we have shown that the gravitational forces have no influence on the detachment of the bubbles nor on their size even in the presence of gravity.

This study has highlighted the role of surface tension force and its importance on the growth and detachment of bubbles. It acts as an attaching force at the injection nozzle during the bubble growth stage until the formation of the neck. The capillary effects then tend to reduce the diameter of the neck until the pinch-off and cause the detachment of the bubble.

Wall-level analysis is used to describe the motion of the contact line during the bubble growth process and its significant effect on bubble formation. We have demonstrated an influence of the contact line on the size of bubbles formed depending on whether the contact line is fixed or mobile. We have shown that the detachment time is substantially reduced when the contact line is fixed compared to that of a mobile contact line, thus producing smaller size bubbles. The comparative study between the forces applied on the bubble allowed to highlight the significant influence of the contact line.

References

Albadawi, A., Donoghue, D. B., Robinson, A. J., Murray, D. B. & Delauré, Y. M. C. Influence of surface tension implementation in Volume of Fluid and coupled Volume of Fluid with Level Set methods for bubble growth and detachment. Int. J. Multiph. Flow**53**, 11–28 (2013).

Albadawi, A., Donoghue, D. B., Robinson, A. J., Murray, D. B. & Delauré, Y. M. C. On the analysis of bubble growth and detachment at low Capillary and Bond numbers using

Volume of Fluid and Level Set methods. Chem. Eng. Sci.**90**, 77–91 (2013).

Barhate,R.S.,Patil,G., Srinivas,N.D.&Raghavarao,K.S.M.S. Drop formation in aqueous two-phase systems, J. Chromatogr. A 1023, 197–206(2004).

Bari, S. di & Robinson, A. J. Experimental study of gas injected bubble growth from submerged orifices. Exp. Therm. Fluid Sci.**44**, 124–137 (2013).

Bolanos-Jimenez, R., A. Sevilla, and C. Martnez-Bazan. The necking time of gas bubbles in liquids of arbitrary viscosity. Phys. Fluids28, 042105 (2016).

Brackbill, J.U., Zemach, C. &Kothe,D.B. A continuum method for modeling surface tension, J. Comput. Phys. 100, 335–354(1992).

Byakova, A. V., Gnyloskurenko, S. V., Nakamura, T. & Raychenko, O. I. Influence of wetting conditions on bubble formation at orifice in an inviscid liquid: Mechanism of bubble evolution. Colloids Surfaces A Physicochem. Eng. Asp.**229**, 19–32 (2003).

Chen,C.T.,Maa,J.R., Yang, Y.M.&Chang, C.H. Drop formation from flat tip nozzles in liquid–liquid system, Int. Commun. Heat Mass Transfer 28. 681–692(2001).

Corchero, G., Medina, A. & Higuera, F. J. Effect of wetting conditions and flow rate on bubble formation at orifices submerged in water. Colloids Surfaces A Physicochem. Eng. Asp.**290**, 41–49 (2006).

Gordillo, J. M. Axisymmetric bubble collapse in a quiescent liquid pool. I. Theory and numerical simulations. Phys. Fluids20, 112103 (2008).

Greenshields, C. J., OpenFOAM UserGuide, Version 3.0.1. ,December (2015).

Das, A. K. & Das, P. K. Numerical Study of Bubble Formation from Submerged Orifice under Reduced Gravity Condition. Procedia IUTAM**18**, 8–17 (2015).

Davidson,J.F. &Schüler, B.O.G. Bubble formation at an orifice in a viscous liquid, Trans. Inst. Chem. Eng. 38, S105–S115(1960).

Bari, S., Lakehal, D. & Robinson, A. J. A numerical study of quasi-static gas injected bubble growth: Some aspects of gravity. Int. J. Heat Mass Transf.**64**, 468–482 (2013).

Doshi, P., Cohen, I., Zhang,M., Siegel, W.W. Howell, P.&Basaran, O.A. Nager, S.R. Persistence ofmemory in drop breakup: the breakdownof universality, Science 302 1185–1188(2003).

Duhar, G.& Colin, C. Dynamics of bubbles growth and detachment in a viscous shear flow. Phys. Fluids 18, 77–101 (2006).

Forster, H.K.&Zuber, N. Growth of a vapor bubble in superheated liquids. J. Appl. Phys. 25, 474–478 (1954).

Gaddis,E.S. v Vogelpohl,A. Bubble formation in quiescent liquids under constant flow conditions, Chem. Eng. Sci. 41 (1) 97–105(1986).

Garstecki, P.,Fuerstman, M.J., Stone, H.A.&WhitesidesG.M. Formation of droplets and bubbles in a microfluidic T-junction-scaling and mechanism of break-up, Lab Chip, 6 (3), 437–446 (2006).1.

Georgoulas, A., Koukouvinis, P., Gavaises, M. & Marengo, M. Numerical investigation of quasi-static bubble growth and detachment from submerged orifices in isothermal liquid pools: The effect of varying fluid properties and gravity levels. Int. J. Multiph. Flow**74**, 59–78 (2015).

Gerlach, D., Alleborn, N., Buwa, V. & Durst, F. Numerical simulation of periodic bubble formation at a submerged orifice with constant gas flow rate. Chem. Eng. Sci.**62**, 2109–2125 (2007).

Ghaemi, S., Rahimi, P. & Nobes, D.S. The effect of gas-injector location on bubble formation in liquid cross flow. Phys. Fluids.**22**, 1–15 (2010).

Gopala, V. R. & van Wachem, B. G. M. Volume of fluid methods for immiscible-fluid and free-surface flows. Chem. Eng. J.**141**, 204–221 (2008).

Günther, A. Jensen, K.F. Multiphase microfluidics: from flow characteristics to chemical and materials synthesis. Lab Chip, 6 (12), 1487–1503(2006).

Harkins,W.D. &Brown,F.E. The determination of surface tension (free surface energy), and the weight of falling drops: the surface tension of water and benzene by the capillary height method, Journal of the American Chemical Society 41, 499–524(1919).

Hayworth. &Treybal, Drop formation in two-liquid-phase systems, Ind. Eng. Chem. 42, 1174–1181(1950).

Hirt, C. W. & Nichols, B. D. Volume of fluid (VOF) method for the dynamics of free boundaries. J. Comput. Phys.**39**, 201–225 (1981).

Hua, J. &Lou, J., 2007. Numerical simulation of bubble rising in viscous liquid. J. Comput. Phys. 222, 769–795.

Issa, R. Solution of the implicitly discretized fluid flow equations by operator- splitting. J. Comput. Phys. 62, 40–65 (1986).

Javadi, A.,Bastani, D.&Taeibi-Rahni, M. Mass transfer during drop formation on the nozzle: new flow expansion model, AIChE J. 52, 895–910 (2006).

Jobehdar, M. H., Siddiqui, K., Gadallah, A. H. & Chishty, W. A. Bubble formation process from a novel nozzle design in liquid cross-flow. Int. J. Heat Fluid Flow**0**, 1–11 (2016).

Kim,I.,Kamotani, Y.&Ostrach, S. Modeling bubble and drop formation in flowing liquids in microgravity, AIChE J. 40, 19–28(1994).

Kumar,R. A unified approach to bubble and drop formation, Chem. Eng. Sci. 26, 177–184 (1971).

Lesage, F. J. & Marois, F. Experimental and numerical analysis of quasi-static bubble size and shape characteristics at detachment. Int. J. Heat Mass Transf.**64**, 53–69 (2013).

Li, H.Z., Mouline, Y. &Midoux, N., Modelling the bubble formation dynamics in non-Newtonian fluids. Chem. Eng. Sci. 57, 339–346 (2002).

Martin, M., Montes, J.F. &Galan, M.A., 2006. Numerical calculation of shapes and detachment times of bubbles generated from a sieve plate. Chem. Eng. Sci. 61, 363–369.

Nahra, H. K. & Kamotani, Y. Prediction of bubble diameter at detachment from a wall orifice in liquid cross-flow under reduced and normal gravity conditions. Chem. Eng. Sci.**58**, 55–69 (2003).

Notz, P.K., Chen, A.U. &Basaran,O.A. Satellite drops: unexpected dynamics and change of scaling during pinch-off, Phys. Fluids 13, 549–552(2001).

Oguz, H.N. &Prosperetti, A. Dynamics of bubble growth and detachment from a needle. J. Fluid Mech. 257, 111–145 (1993).

Peregrine, D.H., Shaker,G.& Symon,A. The bifurcation of liquid bridges, J. Fluid Mech. 212 25–39(1990).

Prakash,M.&Gershenfeld, N. Microfluidic bubble logic. Science, 315 (5813), 832–835(2007).

Quan, S. & Hua, J. Numerical studies of bubble necking in viscous liquids. Phys. Rev. E - Stat. Nonlinear, Soft Matter Phys.**77**, 1–11 (2008).

Rao, E.V.L.N., Kumar,R.&Kuloor, N.R. Drop formation studies in liquid–liquid systems, Chem. Eng. Sci. 21, 867–880(1966).

Richards, J.R.,Beris, A.N. &Lenhoff, A.M. Drop formation in liquid–liquid systems before and after jetting, Phys. Fluids 7, 2617–2630(1995).

Riznic, J., Kojasoy, G. &Zuber, N. On the spherically symmetric phase change. (1999)

Scheele, G.F. &Meister. B.J.Drop formation at low velocities in liquid–liquid systems. Part I. Prediction of drop volume, AIChE J. 14, 9–15(1968).

Scheele, G.F. &MeisterB.J. Drop formation from cylindrical jets in immiscible liquid systems, AIChE J. 15, 700–706(1969).

Scriven, L.E. On the dynamics of phase growth. Chem. Eng. Sci. 10, 1–13 (1959).

Shi, X.D., Brenner, M.P. &Nagel, S.R. A cascade of structure in a drip falling from a faucet, Science 265 219–222(1994).

Shui, L., Eijkel, J.C. van den Berg,A. Multiphase flow in microfluidic systems - control and applications of droplets and interfaces. Adv. Colloid Interface, 133 (1), 35–49(2007).

Teresaka, K., &Tsuge, H., 1993. Bubble formation under constant-flow conditions. Chem. Eng. Sci. 48, 3417–3422.

Thoroddsen, S. T., Etoh, T. G., &Takehara, K. Experiments on bubble pinch-off. Phys. Fluids**19**, 042101(2007).

Timgren, A., Trägårdh, G.&Trägårdh, C. Application of the PIV technique to measurements around and inside a forming drop in a liquid–liquid system, Exp. Fluids 44, 565–575 (2008).

Vafaei, S. & Wen, D. Bubble formation on a submerged micronozzle. J. Colloid Interface Sci.**343**, 291–297 (2010).

Van Stralen, S.J.D., Cole, R.,Sluyter,&W.M. Sohal, M.S. Bubble growth rates in nucleate boiling of water at subatmospheric pressures. Int. J. Heat Mass Transfer 18 (5), 655–669 (1975).

Vazquez, A., Leifer, I. & Sánchez, R. M. Consideration of the dynamic forces during bubble growth in a capillary tube. Chem. Eng. Sci.**65**, 4046–4054 (2010).

Wang, W., Ngan, K. H., Gong, J. & Angeli, P. Observations on single drop formation from a capillary tube at low flow rates. Colloids Surfaces A Physicochem. Eng. Asp.**334**, 197–202 (2009).

Wilkes, E.D., Phillips, S.D. &Basaran, O.A. Computational and experimental analysis of dynamics of drop formation, Phys. Fluids 11, 3577–3598(1999).

Wu, Y. &Gidaspow, D. Hydrodynamic simulation of methanol synthesis in gas–liquid slurry bubble column reactors. Chem. Eng. Sci. 55 (3), 573–587(2000).

Xu, J.H., Luo, G.S., Chen, G.G. &Wang, J.D.Experimental and theoretical approaches on droplet formation froma micrometer screen hole, J. Membr. Sci. 266, 121–131(2005).

Zhang, L. &Shoji, M., Aperiodic bubble formation from a submerged orifice. Chem. Eng. Sci. 56, 5371–5381(2001).

Zeguai, S., Chikh, S., Tadrist, L.Experimental Study of Two-Phase Flow Pattern Evolution in a Horizontal Circular Tube of Small Diameter in Laminar Flow Conditions. Int. J. of Multiphase flow. 55, 99-110(2013).